

Finite-momentum Cooper pairing in proximitized altermagnets

Received: 26 July 2023

Accepted: 8 February 2024

Published online: 27 February 2024

 Check for updatesSong-Bo Zhang ^{1,2,3}✉, Lun-Hui Hu ^{4,5,6}✉ & Titus Neupert³

Finite-momentum Cooper pairing is an unconventional form of superconductivity that is widely believed to require finite magnetization. Altermagnetism is an emerging magnetic phase with highly anisotropic spin-splitting of specific symmetries, but zero net magnetization. Here, we study Cooper pairing in metallic altermagnets connected to conventional *s*-wave superconductors. Remarkably, we find that the Cooper pairs induced in the altermagnets acquire a finite center-of-mass momentum, despite the zero net magnetization in the system. This anomalous Cooper-pair momentum strongly depends on the propagation direction and exhibits unusual symmetric patterns. Furthermore, it yields several unique features: (i) highly orientation-dependent oscillations in the order parameter, (ii) controllable $0-\pi$ transitions in the Josephson supercurrent, (iii) large-oblique-angle Cooper-pair transfer trajectories in junctions parallel with the direction where spin splitting vanishes, and (iv) distinct Fraunhofer patterns in junctions oriented along different directions. Finally, we discuss the implementation of our predictions in candidate materials such as RuO_2 and KRu_4O_8 .

Cooper pairs are fundamental to the phenomenon of superconductivity and play a vital role in the emergence of its unique properties such as perfect electrical conductivity and Meissner effect¹. Conventionally, Cooper pairs consist of electrons with opposite spins and momenta, thus carrying zero total momentum. The interplay of magnetism and superconductivity gives rise to various intriguing and exotic phenomena, making it one of the current research focuses in condensed matter physics^{2–8}. In particular, a finite magnetization can induce Cooper pairs with finite center-of-mass momentum^{9,10}, which can be observed, e.g., in a 2D superconductor subjected to an applied magnetic field^{11–14} or a ferromagnetic medium close to a superconductor^{15–20} (see Fig. 1a, c for an illustration). The finite-momentum pairing manifests as an oscillating order parameter in real space. In Josephson junctions, the ground state usually has no phase difference across the junction and is referred to a 0 -junction. However, the finite magnetization may produce an intrinsic π phase difference,

forming a so-called π -junction^{21,22}. Notably, a switchable π state of Josephson junction holds important applications in superconducting circuits and qubits^{23–25}.

While it is widely believed that finite-momentum Cooper pairing requires a non-zero net magnetization, in this work, we challenge this by revealing that magnetic systems with zero net magnetization can after all support Cooper pairs with finite momentum by sacrificing uniformity. As a proof-of-concept, we take altermagnetic metals as an example. Altermagnetism is an emerging magnetic phase beyond conventional ferromagnetism and antiferromagnetism and features highly anisotropic spin splitting in electronic bands with specific symmetry but zero net magnetization (e.g., a *d*-wave-like magnetism)^{26–32} (see Fig. 1b). This novel phase may be caused by Fermi-surface instabilities^{26–28}. It can also arise directly from symmetries of the crystal potential and does not require strongly correlated systems^{29,31,32}. It breaks the combined symmetry of translation and C_2 spin rotation that flips the spin (which is

¹Hefei National Laboratory, Hefei, Anhui 230088, China. ²International Center for Quantum Design of Functional Materials (ICQD), University of Science and Technology of China, Hefei, Anhui 230026, China. ³Department of Physics, University of Zürich, Winterthurerstrasse 190, 8057 Zürich, Switzerland.

⁴Department of Applied Physics, Aalto University School of Science, FI-00076 Aalto, Finland. ⁵Center for Correlated Matter and School of Physics, Zhejiang University, Hangzhou 310058, China. ⁶Department of Physics and Astronomy, The University of Tennessee, Knoxville, TN 37996, USA.

✉ e-mail: songbozhang@ustc.edu.cn; hu.lunhui.zju@gmail.com

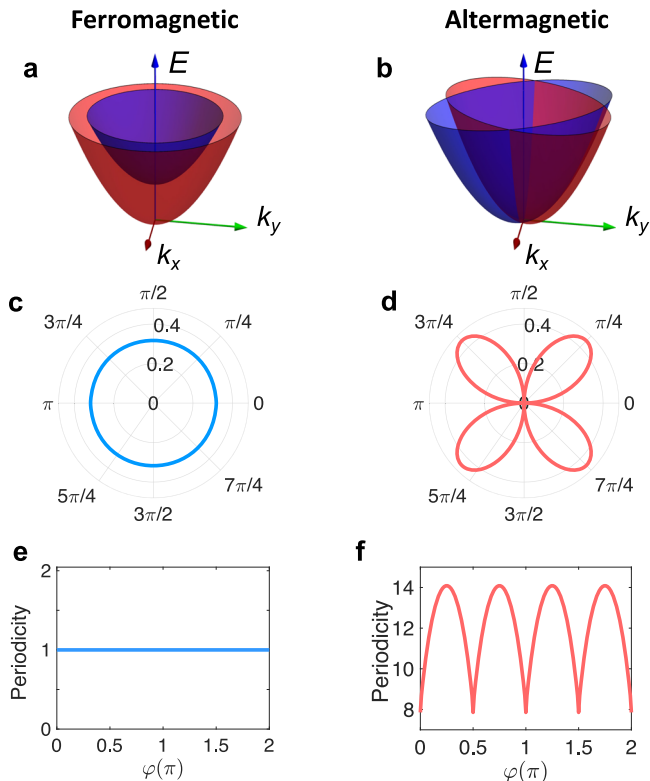


Fig. 1 | Contrast of finite-momentum pairing in the ferromagnetic and altermagnetic metals. **a, b** Schematics of the band structures of the ferromagnet and the altermagnet, respectively. Blue and red distinguish the two bands of opposite spins. In the calculation for the ferromagnet, we replace $Jk_x k_y s_z$ with a constant magnetization Js_z in Eq. (1) and consider the long-wavelength limit with spatial rotation symmetry in the normal kinetic energy part. **c** Polarplots of the Cooper-pair momentum q as a function of the propagation direction θ in the ferromagnet. **d** The same as (c) but for the altermagnet. The Cooper-pair momentum is strongly anisotropic and vanishes when propagating along a crystalline axis ($\theta = n\pi/2$ with $n \in \{0, 1, 2, 3\}$). **e** Periodicity (in units of $\pi\hbar/E_{ex}$) of the order parameter with respect to y'/v_F as a function of junction orientation φ in the ferromagnet. y' is the distance from the ferromagnet-superconductor interface, v_F is the Fermi velocity and E_{ex} is the exchange energy of the ferromagnet. **f** Periodicity with respect to $\sqrt{\mu}y'$ as a function of φ in the altermagnetic junction. Other parameters are $t=1$ and $J=0.8$.

required for classical collinear antiferromagnets), but preserves a joint symmetry of spatial rotation and C_2 spin rotation. Notably, altermagnetism has been found to exhibit many intriguing properties and functionalities, such as high-efficiency spin current generation³³, giant tunneling magnetoresistance^{34,35} and anomalous Hall effect³⁶, thereby arousing considerable theoretical and experimental interest. Importantly, it has also been discovered in a growing number of collinear magnetic materials^{28–32,36–41} including RuO_2 ^{28,31}, KRu_4O_8 ³¹, $\kappa\text{-Cl}$ ^{29,37} and Mn_5Si_3 ⁴².

In this work, we study systematically the Cooper pair propagators in an altermagnetic metal and the superconducting proximity effect in planar junctions formed by the altermagnet and conventional s -wave superconductors. Remarkably, we find that the proximity-induced Cooper pairs in the altermagnet receive a finite momentum although the system has zero net magnetization. Such anomalous Cooper-pair momentum strongly depends on the propagation direction of the Cooper pair. It exhibits a highly anisotropic symmetric pattern and vanishes in particular directions (see Fig. 1d), as inherited from the intrinsic anisotropic spin splitting of the altermagnet. Moreover, it manifests several unique and measurable features: first, it gives rise to damped periodic oscillations in the order parameter as a function of doping in the altermagnet or

distance from the altermagnet-superconductor (AM-SC) interface, which occurs for any junction orientation. The periodicity and decaying behavior depend strongly on the junction orientation, contrasting with those in ferromagnetic junctions (see Fig. 1e, f).

Second, the finite-momentum pairing results in anomalous $0-\pi$ transitions in a planar Josephson junction by modulating the doping in the altermagnet, the length or orientation of the junction, which occurs in the absence of a net magnetization. Note that a π -junction may also occur in Josephson junctions formed by antiferromagnets, which however requires odd layers of the antiferromagnet and thus a finite magnetization⁴³. Third, we find that when the junction is along the direction where the spin splitting of the altermagnet is maximized, the superconducting transport is dominated by Cooper pairs moving along the junction direction. Whereas when the junction is along the direction where the spin splitting vanishes, the transport is dominated by Cooper pairs moving at large oblique angles from the junction direction. As a result, when reducing junction width, the current density in the former junction remains qualitatively unchanged, whereas it changes dramatically in the latter junction. To our knowledge, this effect has not been seen in previously known ferromagnetic and antiferromagnetic counterparts. Finally, we demonstrate that the distinct dominant Cooper-pair transfer trajectories in junctions oriented along different directions also result in different Fraunhofer interference patterns when subjected to an external magnetic field.

Results

Effective model

In altermagnets, the spin splitting of electronic bands changes sign in momentum space and the net magnetization is zero due to the presence of rotational symmetry. To illustrate our main results, we consider an altermagnetic metal with d -wave-like magnetism in two dimensions (2D). This can be realized, for instance, in thin films of RuO_2 and KRu_4O_8 ³². In the long-wavelength limit, the altermagnet can be described by³⁵

$$\mathcal{H}(\mathbf{k}) = t(k_x^2 + k_y^2) + Jk_x k_y s_z, \quad (1)$$

where $\mathbf{k} = (k_x, k_y)$ is the wavevector, the Pauli matrices $\{s_x, s_y, s_z\}$ act on spin space, t parameterizes the usual kinetic energy and is taken to be the unit of energy, i.e., $t=1$, J is the strength of altermagnetic order arising from the anisotropic exchange interaction^{31,32}. The spin component in the z -direction is a good quantum number. Note, however, that our main results of finite-momentum pairing, order parameter and Josephson supercurrent, discussed below, hold for the case with the spin polarization in other directions. Without loss of generality, we work in the eigenbasis of s_z . The model respects $[C_2||C_{4z}]$ symmetry, i.e., a four-fold rotation in real space $((x, y) \rightarrow (y, -x))$ together with a two-fold rotation in spin space $((\uparrow, \downarrow) \rightarrow (\downarrow, \uparrow))$, which is indicated by the relation $s_y \mathcal{H}^*(k_x, k_y) s_y = \mathcal{H}(k_y, -k_x)$. Thus, the system has zero net magnetization. Moreover, the two spin-polarized bands of the model are given by $\epsilon_{\eta}(\mathbf{k}) = t(k_x^2 + k_y^2) + \eta J k_x k_y$, where $\eta = \pm 1$ distinguishes spin-up and spin-down, respectively. It has a band structure similar to those for KRu_4O_8 and RuO_2 ^{31,33} (see Fig. 1b). The spin splitting ($Jk_x k_y$) is highly anisotropic and vanishes along the k_x - and k_y -axes, leading to the d -wave-like magnetism.

We note that the direction of the altermagnetic order may deviate from the crystal axis by an angle α , which can be described by rewriting the altermagnetic term as $J[\cos(2\alpha)k_x k_y + \sin(2\alpha)(k_x^2 - k_y^2)/2]s_z$ in Eq. (1). This deviation will only cause an angle shift of 2α in the propagation direction dependence of the Cooper-pair momentum and hence in the junction orientation dependence of the order parameter and Josephson supercurrent. It does not alter our main results qualitatively. For concreteness, we consider $\alpha=0$ and focus on the realistic case with $|J| \lesssim 1$ in the following.

Finite Cooper-pair momentum

In a ferromagnetic metal with proximity-induced superconductivity, the Fermi surface splitting of opposite spins leads to a momentum of Cooper pairs, which is nonzero in any direction (Fig. 1c). We ignore spin-orbit coupling which is typically small in ferromagnetic systems. In contrast, because of the sign-changing nature of spin splitting and vanishingly small net magnetization, unique physics arises in the altermagnet with superconductivity, which we demonstrate numerically and analytically below.

We analyze the Cooper-pair propagator⁴⁴ to study finite-momentum pairing and supercurrents induced in the altermagnet. We consider *s*-wave spin-singlet pairing, which is the case most easily realized experimentally. The Cooper-pair propagator, i.e., the simultaneous propagation of two electrons with opposite spins from one position \mathbf{r}_1 to another position \mathbf{r}_2 at zero temperature, can be calculated as the Cooperon bubble diagram⁴⁵, yielding

$$D(\mathbf{r}_2; \mathbf{r}_1) = \frac{(J_+ J_-)^{3/2}}{\pi^2 r^2 (J_+ + J_-)} (e^{iqr} + e^{-iqr}). \quad (2)$$

where $J_{\pm} = 1/\sqrt{2 \pm J \sin(2\theta)}$, θ is the angle between the propagation direction $\hat{\mathbf{r}}$ and the *x*-axis, $q = \sqrt{2\mu}(J_+ - J_-)$, and μ is the chemical potential of the altermagnet and tunable by a gate voltage. We have denoted by $\mathbf{r} = \mathbf{r}_2 - \mathbf{r}_1$ the displacement of Cooper pair. We provide more details of derivation in the Methods and Supplementary Information⁴⁵.

Strikingly, we observe a finite momentum q of the Cooper pair from the Cooper-pair propagator in Eq. (2). The Cooper-pair momentum comes in pairs with opposite values ($q, -q$), due to the rotational symmetry of the system. Moreover, it exhibits a fourfold rotational symmetry in the propagation direction θ , inherited from the altermagnet. Its magnitude is maximized when the propagation is diagonal to the crystalline axes, i.e., $\theta = \pi/4 + n\pi/2$ with $n \in \{0, 1, 2, 3\}$, whereas vanishes when the propagation is along a crystalline axis, i.e., $\theta = n\pi/2$ (see Fig. 1d). For small $|J| \ll 1$, q is approximately

$$q \approx J\sqrt{\mu} \sin(2\theta) = 2J\sqrt{\mu}xy/r^2. \quad (3)$$

Note that the Cooper-pair momentum occurs in the absence of a net magnetization and is proportional to the square root of the chemical potential $\sqrt{\mu}$ in the altermagnet, in sharp contrast to that in ferromagnets which requires a finite magnetization and decreases with increasing μ ^{2,15,16}. As a result of this anomalous anisotropic momentum, the Cooper pair exhibits damped oscillations as it moves in real space, which is sensitively dependent on the propagation direction. This anisotropic behavior further gives rise to the unique features in the proximity-induced order parameter, Josephson supercurrent, and transfer trajectories of Cooper pairs in junction systems, as we illustrate below.

Proximity-induced order parameter

Equipped with the Cooper-pair propagator, we first study the order parameter induced in the altermagnet connected to an *s*-wave superconductor. To this end, we consider a planar AM-SC junction with the interface at $y' = 0$ along the x' -direction, as sketched in the inset of Fig. 2a. The coupling of the superconductor and altermagnet λ is constant along the interface. Here, the superscript \prime indicates that the interface coordinate x' is rotated by an arbitrary angle φ from the crystalline *x*-axis of the altermagnet. The resulting local order parameter can be calculated from the Cooper-pair propagator as

$$\langle |\Psi(\mathbf{r}')| \rangle = \lambda \int_{-W/2}^{W/2} dx'_1 D(\mathbf{r}'; x'_1, 0), \quad (4)$$

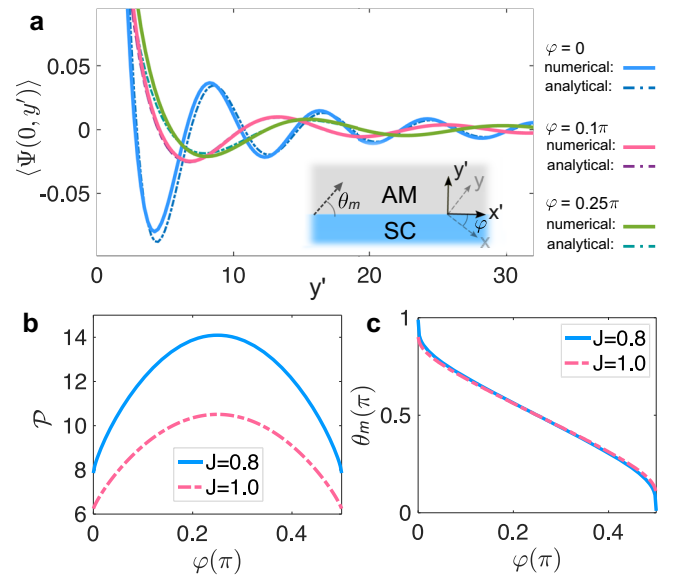


Fig. 2 | Local order parameter near the altermagnet-superconductor (AM-SC) interface. **a** $\langle |\Psi(0, y')| \rangle$ (in units of λ/π^2) as a function of distance y' from the superconductor for junction orientations $\varphi = 0, 0.1\pi$, and 0.25π , respectively. We take $J = 0.8$ for illustration. The dashed curves are the plots of the formula in Eq. (5). Inset depicts the AM-SC junction with the interface at $y' = 0$ along x' -direction. **b** Periodicity \mathcal{P} in $\langle |\Psi(0, y')| \rangle$ with respect to $\sqrt{\mu}y'$ as a function of φ . **c** Angle θ_m of dominant propagation trajectories [sketched in the inset of (a)] as a function of φ . Other parameters are $\mu = 1.0$ and $W = 1000$.

where $\mathbf{r}' = (x', y')$ and W is the junction width. We have ignored the side boundary effect, which is justified for wide junctions $W \gg y'$. For large widths and chemical potentials, $W \gg y' \gg 1/(\sqrt{\mu})$, we find that $\langle |\Psi(\mathbf{r}')| \rangle$ becomes independent of W and position x' along the interface⁴⁵. However, it exhibits damped oscillates around zero with distance y' from the interface, as shown in Fig. 2a. These behaviors occur for any junction orientation. Under these considerations, we derive $\langle |\Psi(\mathbf{r}')| \rangle \approx \langle |\Psi(0, y')| \rangle$ as

$$\langle |\Psi(\mathbf{r}')| \rangle \approx \frac{\lambda \Upsilon_{\theta_m}}{(y')^{3/2} \mu^{1/4}} \cos\left(\mathcal{F}_{\theta_m} \sqrt{\mu}y' + \frac{\pi}{4}\right), \quad (5)$$

where $\Upsilon_{\theta} = (2J_+ J_- / \pi)^{3/2} / [(J_+ + J_-) |\partial^2 \mathcal{F}_{\theta} / \partial \theta^2|^{1/2}]$, $J_{\pm} = 1/\sqrt{2 \pm J \sin(2\theta' + 2\varphi)}$ and $\mathcal{F}_{\theta} = \sqrt{2} \csc \theta' (J_- - J_+)$. The angle θ_m is given by the minimum point of \mathcal{F}_{θ} . Physically, it is the angle of the Cooper-pair trajectory whose propagator dominates the integral in Eq. (4). Particularly, $\theta_m = \pi/2$ indicates that the dominant trajectory is normal to the AM-SC interface, while $\theta_m = 0$ (or π) indicates that the dominant trajectory is approximately parallel to the interface. We discuss this picture in more detail later. We provide more details of derivation in the Supplementary Information⁴⁵.

From Eq. (5), we see that the amplitude of $\langle |\Psi(\mathbf{r}')| \rangle$ decays from the AM-SC interface as $\sim (y')^{-3/2}$. This decay stems from the fact the Cooper-pair propagator decays with propagation distance r' as $\sim (r')^{-2}$ [cf. Eq. (2)] and from the strong interference between the Cooper-pair propagators from the superconductor. The magnitude also decreases slowly as $\sim \mu^{-1/4}$ due to the interference between the propagators.

On top of the decay, $\langle |\Psi(\mathbf{r}')| \rangle$ oscillates periodically as $\sqrt{\mu}y'$ increases. The periodicity can be written as

$$\mathcal{P} = 2\pi / |\mathcal{F}_{\theta_m}|. \quad (6)$$

It decreases monotonically with increasing $|J|$. More interestingly, \mathcal{P} increases monotonically as we rotate the junction orientation from

$\varphi = 0$ to $\pi/4$, as shown in Fig. 2b. At $\varphi = 0$, we find that the propagator dominating $\langle |\Psi(\mathbf{r}')| \rangle$ moves in a trajectory nearly parallel to the interface, i.e., $\theta_m \approx 0$. Hence, we have $\mathcal{F}_{\theta_m} = -J$. At $\varphi = \pi/4$, we find instead $\theta_m = \pi/2$, indicating that the dominant propagator moves in the trajectory normal to the AM-SC interface. Accordingly, $\mathcal{F}_{\theta_m} = \sqrt{2}/(2+J) - \sqrt{2}/(2-J) \approx -J/2$. Thus, we have $\mathcal{P}|_{\varphi=\pi/4}/\mathcal{P}|_{\varphi=0} \approx 2$. $\langle |\Psi(\mathbf{r}')| \rangle$ oscillates more rapidly in junctions along a crystalline axis ($\varphi = 0$) than that diagonal to crystalline axes ($\varphi = \pi/4$). These behaviors are well corroborated by numerical calculations in Fig. 2a. It is also worth noting that $\langle |\Psi(\mathbf{r}')| \rangle$ is a periodic function of junction orientation φ with a period $\pi/2$. For given large distance y' and filling in the altermagnet, $\langle |\Psi(\mathbf{r}')| \rangle$ even oscillates around zero with φ within a period. This angular dependence of the order parameter is a direct consequence of the anisotropic momentum of Cooper pairs in the altermagnet [cf. Eq. (3)] and is one of the central predictions in this work. It is generic and independent of the details of the superconductor and junction interface.

Anomalous 0- π transitions in the supercurrent

The unique finite-momentum pairing in the altermagnet also manifests as interesting transport signatures in Josephson junctions. We consider a planar Josephson junction formed by sandwiching the altermagnet with length L by two superconductors along the y' -direction. Similar to the AM-SC junction, we assume constant coupling amplitudes λ_j (with $j \in \{1, 2\}$) along each interface, $\lambda_j(x') = \lambda_j e^{i\phi_j}$, where ϕ_j is the pairing phase in the j -th superconducting lead. The supercurrent can be evaluated as the derivative of free energy with respect to the pairing phase difference $\delta_\phi = \phi_1 - \phi_2$ across the junction. In terms of Cooper-pair propagators, the δ_ϕ -dependent part of free energy can be written as⁴⁵

$$F_{\delta_\phi} = -4\lambda_1\lambda_2 \int dx'_1 dx'_2 \operatorname{Re} \left[e^{i\delta_\phi} D(x'_2, L; x'_1, 0) \right]. \quad (7)$$

Plugging Eq. (2) into Eq. (7), we obtain the supercurrent as $I_s(\delta_\phi) = (e/h)\partial F_{\delta_\phi}/\partial \delta_\phi = I_c \sin(\delta_\phi)$, where the critical current reads

$$I_c = \frac{4e}{\hbar} \lambda_1 \lambda_2 \int_{-W/2}^{W/2} dx'_1 dx'_2 D(x'_2, L; x'_1, 0). \quad (8)$$

A positive I_c corresponds to a 0-junction, whereas a negative I_c indicates a π -junction where the system has an intrinsic π phase difference across the junction at the ground state. Here, we ignore the correction from side boundary reflections. This is justified for $L \lesssim W$, as we show in the Supplementary Information⁴⁵. For large widths and chemical potentials $W \gg L \gg 1/(\sqrt{\mu})$, we can evaluate $\int dx'_1 D(x', L; x'_1, 0)$ in a similar way as the order parameter. It turns out to be constant in x' . This allows us to find I_c analytically as

$$I_c = \frac{4e}{\hbar} \frac{\lambda_1 \lambda_2 W}{L^{3/2} \mu^{1/4}} \Upsilon_{\theta_m} \cos \left(\mathcal{F}_{\theta_m} \sqrt{\mu} L + \frac{\pi}{4} \right). \quad (9)$$

The agreement between the formula in Eq. (9) and numerical calculations is shown in Fig. 3. It is interesting to note that Eq. (9) takes the same form as the order parameter in the altermagnet, cf. Eq. (5). This suggests that the measurement of I_c , as a function of junction length, chemical potential, and junction orientation can give access to the information about the proximity-induced order parameter, such as its dependence on position (measured from the AM-SC interface), chemical potential and junction orientation.

Strikingly, I_c exhibits pronounced oscillations around zero as a function of junction length L and chemical potential μ in the altermagnet, as shown in Fig. 3a, c. The periodicity in L is given by $\mathcal{P}_y = 2\pi/(\sqrt{\mu}\mathcal{F}_{\theta_m})$, while the periodicity in $\sqrt{\mu}$ reads $\mathcal{P}_\mu = 2\pi/(L\mathcal{F}_{\theta_m})$. They are the same as those in the order parameter. Thus, similarly, I_c oscillates more rapidly in junctions along a crystalline axis where the

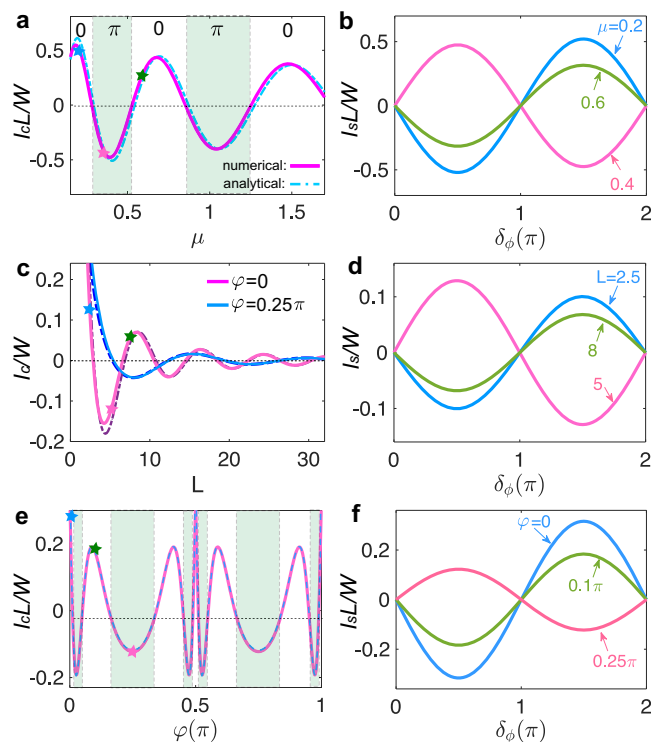


Fig. 3 | Josephson 0- π transition. **a** Critical supercurrent density $I_c L/W$ (I_c is in units of $4e\lambda_1\lambda_2/\pi^2\hbar$) as a function of μ for $\varphi = 0$ and $L = 20$. The dashed curve is the plot of Eq. (9) with the same parameters. I_c oscillates around 0 as L increases. The light green shadows represent the π -junction regions as indicated. **b** Current-phase relation for $\mu = 0.2, 0.4$ and 0.6 , respectively [marked by the colored stars in (a)]. **c** $I_c L/W$ as a function of junction length L for $\varphi = 0$ and $\pi/4$, respectively. We take $\mu = 1$ for illustration. The dashed curves are the plots of Eq. (9) for $\varphi = 0$ and $\pi/4$, respectively. **d** Current-phase relation for $L = 2.5, 5$, and 8 , respectively [marked by the colored stars in (c)]. **e** $I_c L/W$ as a function of φ for $\mu = 1$ and $L = 25$. The dashed curve is the plot of Eq. (9) with the same parameters. The light green shadows represent the π -junction regions. **f** Current-phase relation for $\varphi = 0, 0.1\pi$ and 0.25π , respectively [marked by the colored stars in (e)]. Other parameters are the same as Fig. 2 for all plots.

spin splitting of the altermagnet vanishes. In addition, I_c is a periodic function of junction orientation φ with period $\pi/2$. For large given L and μ , we also observe oscillations of I_c around zero as a function of φ within a period (see Fig. 3e). The oscillations become denser when φ is close to $n\pi/2$ with n being an integer because \mathcal{F}_{θ_m} changes faster there. Experimentally, one could fabricate curved devices with a series of superconducting lead pairs, similar to those used for anisotropic magnetoresistance measurements^{46,47}, which allows an effective rotation of the junction orientation.

As discussed earlier, positive (negative) I_c corresponds to a 0 (π) state of the Josephson junction. These oscillations indicate 0- π transitions of the Josephson junction when we vary the junction length L , chemical potential μ , or junction orientation φ , as shown in Fig. 3b, d, f. These results are also independent of the details of the s -wave superconductors and AM-SC interfaces (note that the interface couplings $\lambda_{1,2}$ only alter the magnitude of the current). It is also worth noting that the π -junction and 0- π transitions in the altermagnetic junction occur in the absence of a net magnetization. This is again in sharp contrast to ferromagnetic or antiferromagnetic junctions where a π -junction requires a finite net magnetization^{15–20,43,48,49}.

Dominant Cooper-pair transfer trajectory

Our analytical result in Eq. (9) illustrates not only the anomalous 0- π transitions, but also intriguing features in the main trajectory direction of Cooper pairs transferring across the junction. The dominant Cooper-

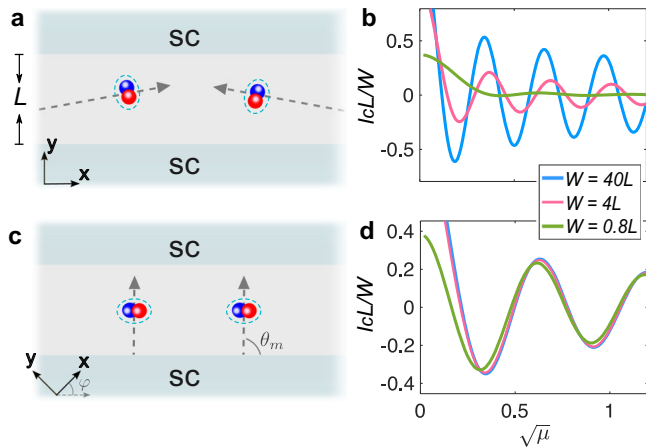


Fig. 4 | Dominant transfer trajectory of Cooper pairs. **a** Schematic of Cooper-pair transfer in junctions along x - or y -axis. The superconducting transport is dominated by Cooper pairs moving at large oblique angles (sketched by dashed arrows). **b** $I_c L/W$ as a function of $\sqrt{\mu}$ for $\varphi = 0$ and $W = 40L$, $4L$ and $4L/5$, respectively. **c** Schematic of Cooper-pair transfer in junctions along a diagonal (i.e., $[1\bar{1}]$ or $[\bar{1}1]$) direction. The transport is dominated by Cooper pairs moving in the junction direction. **d** $I_c L/W$ as a function of $\sqrt{\mu}$ for $\varphi = \pi/4$ and $W = 40L$, $4L$ and $4L/5$, respectively. In **(b, d)**, $L = 25$ and other parameters are the same as Fig. 2.

pair transfer trajectory is described by the angle θ_m , as we mentioned before. In Fig. 2c, we calculate θ_m as a function of junction orientation φ . We find that θ_m changes monotonically from 0 (or equivalently π) to $\pi/2$ as we rotate the junction from the direction where the splitting of the altermagnetic vanishes (i.e., crystalline axis, $\varphi = n\pi/2$ with $n \in \{0, 1, 2, 3\}$) to the diagonal direction where the spin splitting maximizes (i.e., $\varphi = \pi/4 + n\pi/2$). This indicates that the main transfer direction of Cooper pairs changes substantially. In particular, when the junction is oriented diagonal to the crystalline axes, we find $\theta_m = \pi/2 + n\pi$. Thus, the transport is dominated by Cooper pairs that move in the junction direction (see a sketch in Fig. 4c). In contrast, when the junction is parallel to a crystalline axis, we find $\theta_m = n\pi$. The transport is instead dominated by Cooper pairs that move at large oblique angles from the junction direction (see a sketch in Fig. 4a). We remark that such a large-oblique-angle Cooper-pair transfer is closely associated with the vanishing of Cooper-pair momentum in specific directions and is absent in ferromagnetic or antiferromagnetic junctions.

As a result of the distinct dominant transfer trajectories of Cooper pairs, the transport properties in junctions along and diagonal to the crystalline axes respond differently to the change of junction width W . Specifically, for junctions along a crystalline axis, the amplitude of the current density I_c/W is significantly suppressed by reducing W since fewer Cooper pairs move at large oblique angles. The oscillations in the order parameter and hence $0-\pi$ transitions of the supercurrent are also strongly suppressed for small $W \lesssim L$. In contrast, for junctions diagonal to the crystalline axes, I_c/W is nearly insensitive to the change of W . Accordingly, the oscillations and $0-\pi$ transitions can be observed even for $W \lesssim L$. These results are well confirmed by our numerical calculations in Figs. 4b, d, where we perform the direct integration of x' and x'_1 from $-W/2$ to $W/2$ in Eq. (8).

Fraunhofer interference pattern

Finally, we apply a perpendicular magnetic field B to the Josephson junction and study how it influences the supercurrent. The application of a magnetic field will induce spatial variations in the phase of pairing potentials along the AM-SC interfaces, thus significantly altering the interference between the Cooper-pair propagators and supercurrent across the junction. We provide the details of the calculation in the Supplementary Information⁴⁵.

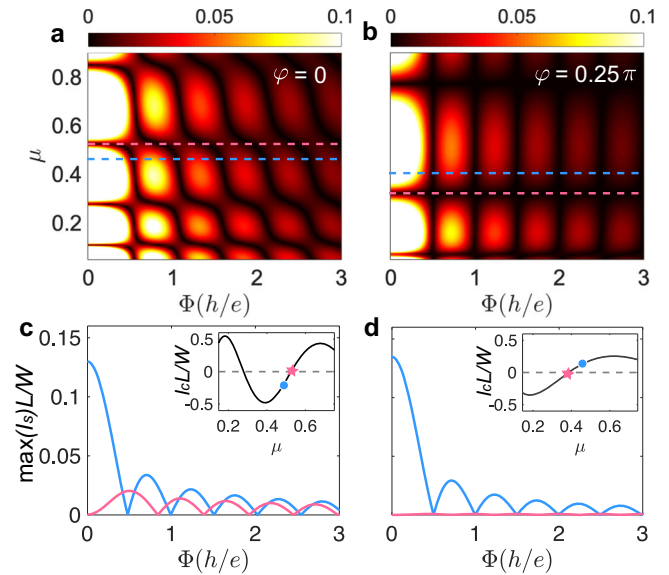


Fig. 5 | Fraunhofer interference patterns. **a** Maximal supercurrent $\max(I_s)$ (I_s is in units of $4e\lambda_1\lambda_2/\pi^2\hbar$) as a function of chemical potential μ and external perpendicular magnetic flux (field) $\Phi = BWL$ (in units of magnetic flux quantum h/e) in a Josephson junction oriented along x - or y -axis. **b** The same as **(a)** but for a junction oriented with $\varphi = \pi/4$. **c** Fraunhofer patterns at a $0-\pi$ transition point (pink) or away from the transition points (blue) in a junction oriented along x - or y -axis. The corresponding chemical potentials are marked by the colored markers in the inset. The two curves correspond to the two dashed line cuts in **(a)**, respectively. **d** The same as **(c)** but for a junction oriented with $\varphi = \pi/4$. Other parameters are the same as Fig. 3.

In Fig. 5, we compute numerically the Fraunhofer interference patterns which measure the maximum supercurrent $\max(I_s)$ in response to the applied magnetic field, for varying chemical potential. It is striking to see that the junctions oriented along the maximum and vanishing Fermi surface spin-splitting directions exhibit distinct Fraunhofer patterns (see Fig. 5a, b). Explicitly, in the junction along the direction where the Fermi surfaces are most split ($\varphi = \pi/4$), we observe a conventional Fraunhofer pattern, in which the maximum supercurrent is located at zero field (see Fig. 5b, d). This feature is similar to that in ordinary Josephson junctions as the dominant Cooper-pair transfer trajectory consistently aligns with the junction direction. In contrast, at the $0-\pi$ transition points of the junction along the direction where the spin-splitting vanishes (i.e., x - or y -axis), a finite supercurrent can be induced and enhanced by the applied magnetic field, as shown in Fig. 5c. This result is closely related to the fact the dominant Cooper-pair propagators are moving at large oblique angles across the junction. Note that in this case, the local critical-current density $j_c(x')$ may significantly vary with the change of the interface coordinate x' , which is different from ordinary planar junctions where Cooper pairs propagate mainly in the junction direction and thus $j_c(x')$ is approximately a constant. These contrast Fraunhofer patterns provide us with another compelling signature to detect the unique superconducting transport properties of the altermagnetic junctions.

Discussion

To summarize, we have shown that Cooper pairs in the altermagnet acquire a finite momentum despite the system having zero net magnetization. This anomalous momentum is highly anisotropic with respect to the direction of Cooper-pair propagation. We have further shown that it gives rise to several unique features: (i) The order parameter oscillates with the gate voltage on the altermagnet and/or with the distance from the superconductor, which depends sensitively on the junction orientation; (ii) In planar Josephson junctions, although there is no net magnetization, $0-\pi$ transitions occur as a function of

Table 1 | Comparison of different approaches to generate finite-momentum Cooper pairing

Systems	Rashba ⁵⁵	Dirac surface states ^{18,19}	Altermagnet (this work)
Finite momentum q	$H_{\parallel}/\sqrt{\alpha_R^2 + \mu^2/m}$	H_{\parallel}/v_F	$\sqrt{2\mu} \sin(2\theta)$
Magnetic field (magnetization)	in-plane field	in-plane field	no field
θ dependence	no	no	yes
Large oblique-angle transport	no	no	yes
μ dependence	large μ , smaller q	no	larger μ , larger q

It summarizes theoretical results (e.g., finite momentum q , requirements of magnetic fields (magnetization), dependence on the chemical potential μ and propagation direction θ , and large oblique-angle transport) for three systems: (1) Rashba superconductor with s -wave pairing under in-plane magnetic field H_{\parallel} , α_R is the Rashba spin-orbit coupling, μ is the chemical potential and m is the effective mass. (2) Dirac surface states with proximity-induced s -wave pairing under in-plane magnetic field H_{\parallel} , v_F is the Fermi velocity. (3) Altermagnet with proximity-induced s -wave pairing.

gate voltage on the altermagnet, length or orientation of the junction; (iii) In junctions parallel to the direction where the spin splitting of the altermagnet vanishes, the superconducting transport is dominated by Cooper pairs moving at large oblique angles away from the junction direction; (iv) Josephson junctions oriented along different directions exhibit distinct Fraunhofer interference patterns in response to external magnetic fields. These results are generic and do not rely on the details of the s -wave superconductors and junction interfaces.

Compared to the previously studied platforms for realizing finite-momentum pairings, such as Rashba superconductors and Dirac surface states with proximity-induced superconductivity, our proposal does not require a magnetic field (or net magnetization). In the altermagnetic system, the Cooper-pair momentum depends substantially on the propagation direction θ and the larger oblique-angle Cooper transfer can dominate the superconducting transport, which does not exist in the ferromagnetic junctions. Additionally, the Cooper-pair momentum exhibits a rather different dependence on the chemical potential μ of the system. We summarize the comparisons between the typical ferromagnetic and altermagnetic systems in Table 1.

There has been a growing number of candidate materials predicted and confirmed as altermagnet. Among them, a prime example is the collinear RuO₂ that has been widely studied theoretically and experimentally^{28,31,36,50–52}. RuO₂ possesses a strong anisotropic spin-splitting (on the eV scale) in the electronic band structure, which has been verified in ARPES experiment recently⁵³. Thin films of RuO₂ have also been realized and, interestingly, with signatures of intrinsic superconductivity^{51,52}. Using typical parameters for this material, $Ja^2 = 1$ eV, $ta^2 = 2.5$ eV, lattice constant $a = 4.5$ Å and doping $\mu = 0.3–0.5$ eV^{28,35}, we estimate the shortest periodicity (at $\varphi = 0$) with respect to the junction length as $\mathcal{P}_y = 2\pi\sqrt{t^3/(\mu J^2)} \sim 16–20$ nm. Thus, it is feasible to observe the oscillations of order parameter and Josephson current in superconducting junctions with lengths longer than 20 nm. Similar to RuO₂, KRu₄O₈ has a d -wave-like altermagnetic order but is described by $J(k_x^2 - k_y^2)s_z/2$ ³¹. It is precisely related to $Jk_x k_y s_z$ by 45-degree rotation about z -axis. The spin splitting maximizes in the k_x - and k_y -axes while vanishes in the $k_x = \pm k_y$ directions. Thus, our results also apply to this material but with swapping the directions parallel and diagonal to the crystal axis. For KRu₄O₈, we take the parameters $ta^2 = 0.05$ eV, $Ja^2 = 0.037$ eV, $a = 9.9$ Å and $\mu = 0.03–0.1$ eV³¹ and estimate the shortest periodicity (at $\varphi = \pi/4$) a $\mathcal{P}_y \sim 6–11$ nm. Therefore, the oscillations could be observed in KRu₄O₈-based junctions with shorter lengths compared to those of RuO₂.

So far, we have focused on the altermagnet metals with d -wave magnetism. Our main results, however, can be easily generalized to other planar altermagnetic metals, e.g., with g - or i -wave magnetism. In particular, we expect pronounced oscillations in the induced order parameter with respect to junction length or doping for any junction orientation. The periodicity of the oscillations is determined by the junction orientation. It is the largest (smallest) when the junction is aligned with the direction where the spin splitting of the altermagnet vanishes (maximizes). In Josephson junctions, anomalous $0-\pi$

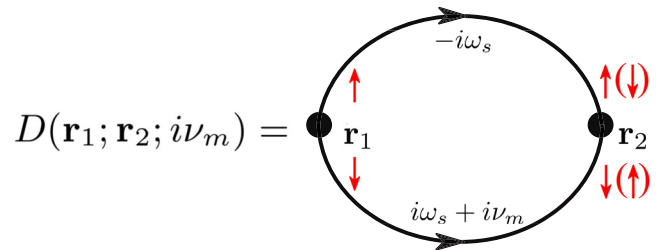


Fig. 6 | Diagram for the propagator for an electron pair. The vertex correction due to the scattering of the electrons is not considered for simplicity. The red arrows indicate opposite spins carried by the electron pair.

transitions occur despite the zero net magnetization. Moreover, the superconducting transport is dominated by Cooper pairs moving at large oblique angles away from the junction direction when the junction is in the direction where the spin splitting vanishes. Thus, the current density becomes sensitive to the width of the junction.

Our work not only sheds light on the exploration and understanding of finite-momentum Cooper pairing in the absence of net magnetization but also uncovers exotic superconducting phenomena in the altermagnet. While our focus lies on the most typical scenario where the altermagnet has the Fermi surfaces at the Γ point and the superconductivity of s -wave singlet pairing, it would be interesting to extend our study to the case with valley degrees of freedom in the altermagnet³² or involving triplet pairing, in particular, in the presence of spin-orbit coupling. It would also be promising to explore topological superconductivity and nonreciprocal superconducting phenomena, such as the diode effect, in altermagnets without net magnetization.

Recently, we became aware of a numerical study⁵⁴ which discusses $0-\pi$ Josephson transitions.

Methods

Cooper-pair propagator

The Cooper-pair propagator describes the simultaneous propagation of two electrons with opposite spins initially from a position \mathbf{r}_1 at time t_1 to another position \mathbf{r}_2 at time t_2 . Using Wick's theorem and the Matsubara formalism, we can evaluate it as a convolution of two electron Green's functions

$$D(\mathbf{r}_1; \mathbf{r}_2; i\nu_m) = \frac{1}{2\beta} \sum_{\omega_s} \text{Tr} [G_0(\mathbf{r}_1, \mathbf{r}_2, -i\omega_s) S_y G_0^T(\mathbf{r}_1, \mathbf{r}_2, i\omega_s + i\nu_m) S_y], \quad (10)$$

where $G_0(\mathbf{r}_1, \mathbf{r}_2, i\omega_s)$ is the non-interacting Matsubara Green's function. It is a 2×2 matrix in the spin basis $(\psi_{\uparrow}, \psi_{\downarrow})$. $\omega_s = (2s+1)\pi k_B T$ and $\nu_m = 2\pi m k_B T$ (with s and m being integers) are Matsubara frequencies for fermions and bosons (here electron pairs). The Feynman diagram for the pair propagator is shown in Fig. 6. Assuming translation symmetry and considering the static limit, the Cooper pair propagator

at zero temperature can be found as

$$D(\mathbf{r}) = D(\mathbf{r}, 0) = \frac{1}{2} \int_0^\infty \frac{d\epsilon d\epsilon'}{2\pi 2\pi} \frac{T(\mathbf{r}, \epsilon, \epsilon') + T(\mathbf{r}, -\epsilon, -\epsilon')}{\epsilon + \epsilon'} \quad (11)$$

where $\mathbf{r} = \mathbf{r}_2 - \mathbf{r}_1$,

$$T(\mathbf{r}, \epsilon, \epsilon') = \text{Tr} \left[g_0(\mathbf{r}, \epsilon) s_y g_0^T(\mathbf{r}, \epsilon') s_y \right], \quad (12)$$

and $g_0(\mathbf{r}, \epsilon)$ is the Fourier transform of the spectral function matrix given by

$$g_0(\mathbf{r}, \epsilon) = \int \frac{d^2\mathbf{k}}{(2\pi)^2} e^{i\mathbf{k}\cdot\mathbf{r}} A_0(\mathbf{k}, \epsilon). \quad (13)$$

For the altermagnet, the spectral function matrix is obtained from the Green's function as

$$\begin{aligned} A_0(\mathbf{k}, \epsilon) &\equiv -2 \text{Im} [G_0^{\text{ret}}(\mathbf{k}, \epsilon)] \\ &= 2\pi \sum_{\eta=\pm 1} \delta(\epsilon - \epsilon_{\mathbf{k}, \eta}) \frac{1 + \eta s_x}{2}, \end{aligned} \quad (14)$$

where $\eta = \pm 1$ distinguishes the two bands $\epsilon_{\mathbf{k}, \eta}$ of opposite spins.

Local order parameter

We derive the order parameter $\langle |\Psi(\mathbf{r}')| \rangle$ by integrating Eq. (4) in the main text. When the interface (junction) width and chemical potential in the altermagnet are large, i.e., $W \gg y' \gg 1/(J\sqrt{\mu})$, the local order parameter $\langle |\Psi(\mathbf{r}')| \rangle$ (not close to the edges at $x' = \pm W/2$) becomes independent of W and position x' along the interface. This result holds for interfaces in any orientation. Thus, it suffices to calculate the order parameter at $x' = 0$ which reads

$$\begin{aligned} \langle |\Psi(0, y')| \rangle &= \frac{2\lambda}{\pi^2} \int_{-W/2}^{W/2} dx'_1 \frac{(J_+ J_-)^{3/2}}{r^2 (J_+ + J_-)} \cos \left[\sqrt{2\mu} r' (J_- - J_+) \right], \end{aligned} \quad (15)$$

where $J'_\pm = 1/\sqrt{2 \pm J \sin(2\theta' + 2\phi)}$. Converting the integral over x' to an integral over the angle θ' (i.e., $dx' = -\csc^2 \theta' d\theta'$), we have

$$\langle |\Psi(0, y')| \rangle = \frac{2\lambda}{\pi^2} \frac{1}{y'} \int_\alpha^{\pi-\alpha} d\theta' \frac{(J_+ J_-)^{3/2}}{J_+ + J_-} \cos(\sqrt{\mu} \mathcal{F}_\theta y'), \quad (16)$$

where $\alpha = \arctan(2y'/W)$ and $\mathcal{F}_\theta = \sqrt{2} \csc \theta' (J_- - J_+)$. For large $y' \gg 1/J\sqrt{\mu}$, the function $\cos(\sqrt{\mu} y' \mathcal{F}_\theta)$ oscillates rapidly as θ' varies. Thus, we can apply the saddle point approximation to the integral over θ' and obtain the analytical result in Eq. (5).

Josephson supercurrent

We derive the formula for Josephson supercurrent. The pairing interaction of the planar Josephson junction can be written as

$$H_p = - \int d^2\mathbf{r}' [\Delta(\mathbf{r}') \Psi^\dagger(\mathbf{r}') + \Delta^*(\mathbf{r}') \Psi(\mathbf{r}')], \quad (17)$$

where $\Psi(\mathbf{r}') \equiv \psi_\uparrow(\mathbf{r}') \psi_\downarrow(\mathbf{r}')$ and $\Delta(\mathbf{r}')$ is the pairing potential. We assume

$$\Delta(\mathbf{r}') = \lambda_1(x') \delta(y') + \lambda_2(x') \delta(y' - L), \quad (18)$$

with $|x'| < W/2$ and that the magnitude of $\lambda_j > 0$ (with $j \in \{1, 2\}$) is constant along the superconducting lead, $\lambda_j(x') = \lambda_j e^{i\phi_j}$.

The supercurrent is given by the derivative of the free energy with respect to the pairing phase difference $\delta_\phi = \phi_1 - \phi_2$ across the junction. The free energy contributed by the pairing interaction, $F_p = \langle |H_p| \rangle$,

reads

$$\begin{aligned} F_p = - \int dx' & \left[\lambda_1(x') \langle |\Psi^\dagger(x', 0)| \rangle + \lambda_2(x') \langle |\Psi^\dagger(x', L)| \rangle \right. \\ & \left. + \lambda_1^*(x') \langle |\Psi(x', 0)| \rangle + \lambda_2^*(x') \langle |\Psi(x', L)| \rangle \right]. \end{aligned} \quad (19)$$

Here, $\langle |\Psi(\mathbf{r}')| \rangle$ is the local order parameter, induced from the two superconducting leads by proximity effect. It can be written as $\langle |\Psi(\mathbf{r}')| \rangle = \langle |\Psi(\mathbf{r}')| \rangle_1 + \langle |\Psi(\mathbf{r}')| \rangle_2$ with

$$\begin{aligned} \langle |\Psi(\mathbf{r}')| \rangle_1 &= \int dx'_1 \lambda_1(x'_1) D(\mathbf{r}'; x'_1, 0), \\ \langle |\Psi(\mathbf{r}')| \rangle_2 &= \int dx'_1 \lambda_2(x'_1) D(\mathbf{r}'; x'_1, W). \end{aligned} \quad (20)$$

Plugging Eq. (20) into Eq. (19), the supercurrent $I_s \equiv (e/\hbar) \partial F_p / \partial \delta_\phi$ is found as

$$\begin{aligned} I_s(\delta_\phi) &= -i \frac{2e}{\hbar} \lambda_1 \lambda_2 \int_{-W/2}^{W/2} dx' dx'_1 \\ & \times [e^{i\delta_\phi} D(x', L; x'_1, 0) - e^{-i\delta_\phi} D(x', 0; x'_1, L)] \end{aligned} \quad (21)$$

Exchanging dummy variables, we replace $D(x', 0; x'_1, L)$ by $D(x', L; x'_1, 0)$. Using the fact that the propagator is real-valued, we derive eventually $I(\delta_\phi) = I_c \sin(\delta_\phi)$ with the critical supercurrent given by Eq. (8).

Data availability

The datasets generated during this study are available from the corresponding authors upon request.

Code availability

The custom codes generated during this study are available from the corresponding authors upon request.

References

1. Tinkmann, M. *Introduction to superconductivity*. (Courier Corporation, 2004).
2. Buzdin, A. I. Proximity effects in superconductor-ferromagnet heterostructures. *Rev. Mod. Phys.* **77**, 935 (2005).
3. Bergeret, F. S., Volkov, A. F. & Efetov, K. B. Odd triplet superconductivity and related phenomena in superconductor-ferromagnet structures. *Rev. Mod. Phys.* **77**, 1321 (2005).
4. Keizer, R. S. et al. A spin triplet supercurrent through the half-metallic ferromagnet CrO₂. *Nature* **439**, 825 (2006).
5. Robinson, J., Witt, J. & Blamire, M. Controlled injection of spin-triplet supercurrents into a strong ferromagnet. *Science* **329**, 59 (2010).
6. Linder, J. & Robinson, J. W. Superconducting spintronics. *Nat. Phys.* **11**, 307 (2015).
7. Eschrig, M. Spin-polarized supercurrents for spintronics: a review of current progress. *Rep. Prog. Phys.* **78**, 104501 (2015).
8. Bergeret, F. S., Silaev, M., Virtanen, P. & Heikkilä, T. T. Colloquium: nonequilibrium effects in superconductors with a spin-splitting field. *Rev. Mod. Phys.* **90**, 041001 (2018).
9. Fulde, P. & Ferrell, R. A. Superconductivity in a strong spin-exchange field, *Phys. Rev.* **135**, A550 (1964).
10. Larkin, A. I. & Ovchinnikov, Y. N. Nonuniform state of superconductor. *Zh. Eksp. Teor. Fiz.* **47**, 1136 (1964) [*Sov. Phys. JETP* **20**, 762 (1965)].
11. Uji, S. et al. Vortex dynamics and the Fulde-Ferrell-Larkin-Ovchinnikov state in a magnetic-field-induced organic superconductor. *Phys. Rev. Lett.* **97**, 157001 (2006).
12. Lortz, R. et al. Calorimetric evidence for a Fulde-Ferrell-Larkin-Ovchinnikov superconducting state in the layered organic superconductor-(BEDT-TTF)₂Cu(NCS)₂. *Phys. Rev. Lett.* **99**, 187002 (2007).

13. Zhu, Z. et al. Discovery of segmented Fermi surface induced by Cooper pair momentum. *Science* **374**, 1381 (2021).
14. Wan, P. et al. Orbital Fulde-Ferrell-Larkin-Ovchinnikov state in an Ising superconductor. *Nature* **398**, 672 (2023).
15. Ryazanov, V. V. et al. Coupling of two superconductors through a ferromagnet: evidence for a π junction. *Phys. Rev. Lett.* **86**, 2427 (2001).
16. Kontos, T. et al. Josephson junction through a thin ferromagnetic layer: negative coupling. *Phys. Rev. Lett.* **89**, 137007 (2002).
17. Blum, Y., Tsukernik, A., Karpovski, M. & Palevski, A. Oscillations of the superconducting critical current in Nb-Cu-Ni-Cu-Nb junctions. *Phys. Rev. Lett.* **89**, 187004 (2002).
18. Hart, S. et al. Controlled finite momentum pairing and spatially varying order parameter in proximitized HgTe quantum wells. *Nat. Phys.* **13**, 87 (2017).
19. Chen, A. Q. et al. Finite momentum Cooper pairing in three-dimensional topological insulator Josephson junctions. *Nat. Commun.* **9**, 3478 (2018).
20. Li, C. et al. 4π -periodic Andreev bound states in a Dirac semimetal. *Nat. Mater.* **17**, 875 (2018).
21. Bulaevskii, L., Kuzii, V. & Sobyanin, A. On possibility of the spontaneous magnetic flux in a Josephson junction containing magnetic impurities. *Solid State Commun.* **25**, 1053 (1978).
22. Buzdin, A. I., Bulaevskii, L. & Panyukov, S. Critical-current oscillations as a function of the exchange field and thickness of the ferromagnetic metal (F) in an SFS Josephson junction. *JETP Lett.* **35**, 178 (1982).
23. Mooij, J. et al. Josephson persistent-current qubit. *Science* **285**, 1036 (1999).
24. Ioffe, L. B., Geshkenbein, V. B., Feigel'man, M. V., Fauchere, A. L. & Blatter, G. Environmentally decoupled sds-wave Josephson junctions for quantum computing. *Nature* **398**, 679 (1999).
25. Feofanov, A. et al. Implementation of superconductor/ferromagnet/superconductor π -shifters in superconducting digital and quantum circuits. *Nat. Phys.* **6**, 593 (2010).
26. Wu, C., Sun, K., Fradkin, E. & Zhang, S.-C. Fermi liquid instabilities in the spin channel. *Phys. Rev. B* **75**, 115103 (2007a).
27. Soto-Garrido, R. & Fradkin, E. Pair-density-wave superconducting states and electronic liquid-crystal phases. *Phys. Rev. B* **89**, 165126 (2014b).
28. Ahn, K.-H., Hariki, A., Lee, K.-W. & Kuneš, J. Antiferromagnetism in RuO₂ as d -wave Pomeranchuk instability. *Phys. Rev. B* **99**, 184432 (2019).
29. Naka, M. et al. Spin current generation in organic antiferromagnets. *Nat. Commun.* **10**, 4305 (2019).
30. Šmejkal, L., González-Hernández, R., Jungwirth, T. & Sinova, J. Crystal Hall effect in collinear antiferromagnets. *Sci. Adv.* **6**, aaz8809 (2020b).
31. Šmejkal, L., Sinova, J. & Jungwirth, T. Beyond conventional ferromagnetism and antiferromagnetism: a phase with nonrelativistic spin and crystal rotation symmetry. *Phys. Rev. X* **12**, 031042 (2022a).
32. Šmejkal, L., Sinova, J. & Jungwirth, T. Emerging research landscape of altermagnetism. *Phys. Rev. X* **12**, 040501 (2022b).
33. González-Hernández, R. et al. Efficient electrical spin splitter based on nonrelativistic collinear antiferromagnetism. *Phys. Rev. Lett.* **126**, 127701 (2021).
34. Shao, D.-F., Zhang, S.-H., Li, M., Eom, C.-B. & Tsymbal, E. Y. Spin-neutral currents for spintronics. *Nat. Commun.* **12**, 7061 (2021).
35. Šmejkal, L., Hellenes, A. B., González-Hernández, R., Sinova, J. & Jungwirth, T. Giant and tunneling magnetoresistance in unconventional collinear antiferromagnets with nonrelativistic spin-momentum coupling. *Phys. Rev. X* **12**, 011028 (2022c).
36. Feng, Z. et al. An anomalous Hall effect in altermagnetic ruthenium dioxide. *Nat. Electron.* **5**, 735 (2022).
37. Naka, M. et al. Anomalous Hall effect in κ -type organic antiferromagnets. *Phys. Rev. B* **102**, 075112 (2020).
38. Naka, M., Motome, Y. & Seo, H. Perovskite as a spin current generator. *Phys. Rev. B* **103**, 125114 (2021).
39. Mazin, I. I., Koepf, K., Johannes, M. D., González-Hernández, R. & Šmejkal, L. Prediction of unconventional magnetism in doped FeSb₂. *Proc. Natl. Acad. Sci. USA* **118**, e2108924118 (2021).
40. Gonzalez Betancourt, R. D. et al. Spontaneous anomalous Hall effect arising from an unconventional compensated magnetic phase in a semiconductor. *Phys. Rev. Lett.* **130**, 036702 (2023).
41. Mazin, I. I. Altermagnetism in MnTe: Origin, predicted manifestations, and routes to detwinning. *Phys. Rev. B* **107**, L100418 (2023).
42. Reichlová, H. et al. Macroscopic time reversal symmetry breaking by staggered spin-momentum interaction, <http://arxiv.org/abs/2012.15651>. arXiv:2012.15651.
43. Andersen, B. M., Bobkova, I. V., Hirschfeld, P. J. & Barash, Y. S. $0-\pi$ Transitions in Josephson Junctions with Antiferromagnetic Interlayers. *Phys. Rev. Lett.* **96**, 117005 (2006).
44. Lee, P. A. & Payne, M. G. Pair propagator approach to fluctuation-induced diamagnetism in superconductors-effects of impurities. *Phys. Rev. B* **5**, 923 (1972).
45. See the Supplementary Information for the details of the derivations of the Cooper-pair propagator, local order parameter, Josephson supercurrents, Fraunhofer patterns, and correction from side edge reflection.
46. Dai, Y. et al. Fourfold anisotropic magnetoresistance of L₁₀FePt due to relaxation time anisotropy. *Phys. Rev. Lett.* **128**, 247202 (2022).
47. Wang, R. et al. Colossal Gilbert damping anisotropy in Heusler-alloy thin films. *Adv. Electron. Mater.* **9**, 2300049 (2023).
48. Oboznov, V. A., Bol'ginov, V. V., Feofanov, A. K., Ryazanov, V. V. & Buzdin, A. I. Thickness dependence of the Josephson ground states of superconductor-ferromagnet-superconductor junctions. *Phys. Rev. Lett.* **96**, 197003 (2006).
49. Kawabata, S., Asano, Y., Tanaka, Y., Golubov, A. A. & Kashiwaya, S. Josephson π state in a ferromagnetic insulator. *Phys. Rev. Lett.* **104**, 117002 (2010).
50. Berlijn, T. et al. Itinerant antiferromagnetism in RuO₂. *Phys. Rev. Lett.* **118**, 077201 (2017).
51. Uchida, M., Nomoto, T., Musashi, M., Arita, R. & Kawasaki, M. Superconductivity in uniquely strained RuO₂ films. *Phys. Rev. Lett.* **125**, 147001 (2020).
52. Occhialini, C. A. et al. Strain-modulated anisotropic electronic structure in superconducting RuO₂ films. *Phys. Rev. Mater.* **6**, 084802 (2022).
53. Fedchenko, O. et al. Observation of time-reversal symmetry breaking in the band structure of altermagnetic RuO₂, <http://arxiv.org/abs/2306.02170>. arXiv:2306.02170.
54. Ouassou, J. A., Brataas, A. & Linder, J. dc Josephson effect in altermagnets. *Phys. Rev. Lett.* **131**, 076003 (2023).
55. Dimitrova, O. & Feigel'man, M. V. Theory of a two-dimensional superconductor with broken inversion symmetry. *Phys. Rev. B* **76**, 014522 (2007).

Acknowledgements

We thank Jian Li and Zhe Yuan for helpful discussion. This work was partially carried out at the University of Science and Technology of China (USTC) and Hefei National Laboratory (HFNL). S.-B.Z. acknowledges the support of the start-up funds at HFNL and USTC. L.-H.H. at Aalto is funded by the Jane and Aatos Erkko Foundation and the Keele Foundation as part of the SuperC collaboration. The work was also supported by the European Research Council (ERC) under the European Union's Horizon 2020 research and innovation program (ERC-StGNeupert-757867-PARATOP), the Innovation Program for Quantum Science and Technology (Grant No. 2021ZD0302800), and Anhui Initiative in Quantum Information Technologies (Grant No. AHY170000).

Author contributions

S.-B.Z. and L.-H.H. conceived the project idea. S.-B.Z. performed the calculations and wrote the manuscript with input from L.-H.H. and T.N. All authors contributed to the scientific discussions and manuscript revisions.

Competing interests

The authors declare no competing interests.

Additional information

Supplementary information The online version contains supplementary material available at <https://doi.org/10.1038/s41467-024-45951-3>.

Correspondence and requests for materials should be addressed to Song-Bo Zhang or Lun-Hui Hu.

Peer review information *Nature Communications* thanks the anonymous reviewer(s) for their contribution to the peer review of this work. A peer review file is available.

Reprints and permissions information is available at <http://www.nature.com/reprints>

Publisher's note Springer Nature remains neutral with regard to jurisdictional claims in published maps and institutional affiliations.

Open Access This article is licensed under a Creative Commons Attribution 4.0 International License, which permits use, sharing, adaptation, distribution and reproduction in any medium or format, as long as you give appropriate credit to the original author(s) and the source, provide a link to the Creative Commons licence, and indicate if changes were made. The images or other third party material in this article are included in the article's Creative Commons licence, unless indicated otherwise in a credit line to the material. If material is not included in the article's Creative Commons licence and your intended use is not permitted by statutory regulation or exceeds the permitted use, you will need to obtain permission directly from the copyright holder. To view a copy of this licence, visit <http://creativecommons.org/licenses/by/4.0/>.

© The Author(s) 2024